EMBO reports

scientific report

Structure of the conserved domain of ANAC, a member of the NAC family of transcription factors

Heidi A. Ernst[1], Addie Nina Olsen[2]*, Karen Skriver[2], Sine Larsen[1,3] & Leila Lo Leggio[1+]*

[1]Department of Chemistry, Centre for Crystallographic Studies, University of Copenhagen, Copenhagen Ø, Denmark, [2]Institute of Molecular Biology, University of Copenhagen, Copenhagen K, Denmark, and [3]European Synchrotron Radiation Facility, Grenoble, France

The structure of the DNA-binding NAC domain of *Arabidopsis* ANAC (abscisic-acid-responsive NAC) has been determined by X-ray crystallography to 1.9 Å resolution (Protein Data Bank codes 1UT4 and 1UT7). This is the first structure determined for a member of the NAC family of plant-specific transcriptional regulators. NAC proteins are characterized by their conserved N-terminal NAC domains that can bind both DNA and other proteins. NAC proteins are involved in developmental processes, including formation of the shoot apical meristem, floral organs and lateral shoots, as well as in plant hormonal control and defence. The NAC domain does not possess a classical helix–turn–helix motif; instead it reveals a new transcription factor fold consisting of a twisted β-sheet surrounded by a few helical elements. The functional dimer formed by the NAC domain was identified in the structure, which will serve as a structural template for understanding NAC protein function at the molecular level.

Keywords: NAC domain; transcription factor; DNA binding; abscisic acid response; *Arabidopsis thaliana*; crystal structure

EMBO reports (2004) **5**, 297–303. doi:10.1038/sj.embor.7400093

INTRODUCTION

The NAC protein family comprises a variety of plant proteins that are identifiable by the presence of a highly conserved N-terminal NAC domain, accompanied by diverse C-terminal domains. NAC is an acronym derived from the names of the three genes first described as containing the domain, namely *NAM* (*no apical meristem*), *ATAF1,2* and *CUC2* (*cup-shaped cotyledon*) (Souer *et al*, 1996; Aida *et al*, 1997). NAC proteins appear to be widespread in plants. For example, the genome of *Arabidopsis thaliana* is estimated to contain at least a hundred NAC-encoding genes, whereas no examples have been found thus far in other eukaryotes (The Arabidopsis Genome Initiative, 2000; Riechmann *et al*, 2000). NAC proteins have been implicated in transcriptional control in a variety of plant processes. Functions include involvement in the development of the shoot apical meristem and floral organs, and in the formation of lateral roots (Souer *et al*, 1996; Aida *et al*, 1997; Xie *et al*, 2000). Furthermore, NAC proteins have been implicated in responses to stress and viral infections (Xie *et al*, 1999; Ren *et al*, 2000; Collinge & Boller, 2001).

Several NAC proteins have been shown to function as transcription activators (Ren *et al*, 2000; Xie *et al*, 2000; Duval *et al*, 2002). The DNA-binding ability of two of these proteins, NAC1 and AtNAM, has been localized to the NAC domain, whereas the C-terminal regions constitute transcriptional activation domains (Xie *et al*, 2000; Duval *et al*, 2002). Several NAC genes are hormone inducible (Hoth *et al*, 2002; Xie *et al*, 2002; Greve *et al*, 2003). NAC domains have also been implicated in interactions with other proteins such as viral proteins (Xie *et al*, 1999; Ren *et al*, 2000) and RING finger proteins (Xie *et al*, 2002; Greve *et al*, 2003). For example, interactions between the auxin-inducible NAC1 protein, involved in lateral root formation, and the RING domain protein SINAT5 attenuate the auxin signal through ubiquitination and degradation of NAC1 (Xie *et al*, 2002). Recently, a NAC protein from *Arabidopsis* (ANAC) was identified as an interaction partner of another RING protein (Greve *et al*, 2003). An examination of interactions between different RING domains and ANAC suggested that RING and NAC interactions may also regulate pathways controlled by the plant stress hormone abscisic acid. The nuclear localization of ANAC and its primary structure characteristics are consistent with a role as a transcription factor.

NAC proteins are thus emerging as important proteins in plant development and biology. Here, the first X-ray crystal structure of a NAC domain, the NAC domain of ANAC, is presented. The structure is used to evaluate previous suggestions on function and

[1]Department of Chemistry, Centre for Crystallographic Studies, University of Copenhagen, Universitetsparken 5, DK-2100 Copenhagen Ø, Denmark
[2]Institute of Molecular Biology, University of Copenhagen, Øster Farimagsgade 2A, DK-1353 Copenhagen K, Denmark
[3]European Synchrotron Radiation Facility (ESRF), 6 rue Jules Horowitz, 38000 Grenoble, France
*These authors contributed equally to this work
[+]Corresponding author. Tel: +45 35 32 02 95; Fax: +45 35 32 02 99; E-mail: leila@ccs.ki.ku.dk

Received 20 October 2003; revised 12 December 2003; accepted 16 December 2003; published online 13 February 2004

interactions, including DNA binding by NAC proteins. The structure provides the framework for understanding the functions of NAC proteins at the molecular level.

RESULTS AND DISCUSSION

Overall structure of the ANAC NAC domain

The overall structure of the NAC domain monomer consists of a very twisted antiparallel β-sheet, which packs against an N-terminal α-helix on one side (α1) and one shorter helix α2 on the other side (Fig 1). The remaining part of the structure comprises loops between the main secondary structure elements, with only sporadic and very short stretches of secondary structure, for example a short β-strand (β″), which packs in a parallel fashion to the first β-strand in the antiparallel β-sheet, and a helical turn (α‴) preceding α2. The extreme N-terminal portion, which contains three extra amino acids encoded by the expression vector, is in an extended conformation. Much of this N-terminal tail is poorly defined in the crystal structure, except where it is involved in crystal contacts. The content of observed secondary structure elements is in good agreement (Fig 2) with previous predictions based on sequence and with circular dichroism spectra (Greve *et al*, 2003).

Searches using DALI (Holm & Sander, 1993) and TOPS-based topology searches (http://www.tops.leeds.ac.uk; Gilbert *et al*, 2001) failed to identify close structural homologues. For all the hits found by DALI, structural similarities were limited to the central β-sheet, and the *Z*-score for the best hit was rather low (3.6). None of the TOPS-based topology search hits had a very significant score, and none of the most significant hits was a transcription factor. The architecture of the NAC domain can thus be considered a novel fold for a DNA-binding transcription factor domain.

NAC dimer

Dimerization of DNA-binding domains is common and can function in modulating the DNA-binding specificity (Müller, 2001). Gel filtration studies on the ANAC NAC domain have shown that it forms mostly dimers in solution (Olsen *et al*, 2004). The diffraction data showed evidence of almost perfect non-crystallographic two-fold symmetry axes parallel to *b* and *c* in the crystal, which could both in principle relate the monomers in the biological dimer (Olsen *et al*, 2004). The extensive contacts involving conserved residues in the dimer formed by the NCS axis parallel to *b* strongly suggest that this is the functional dimer (Fig 3A). The interactions between the monomers are summarized in Table 1, and the residues involved are marked in Fig 2. Among the interactions are two prominent salt bridges formed by the conserved Arg 19 and Glu 26 (Fig 3A). A short antiparallel β-sheet is also formed at the dimer interface, with hydrogen bonds between Arg 19(N–H)…Arg 19(C=O) and Tyr 21(N–H)…Gly 17(C=O). Many hydrophobic interactions occur at the monomer–monomer interface, most of which involve residues in a conserved N-terminal block (Fig 2).

There is overall similarity between the two monomers in the dimer (r.m.s.d. 1.27 and 1.25 Å for 137 and 132 Cα atoms in the dicyanoaurate derivative and the native structure, respectively). However, in the highest resolution dicyanoaurate derivative structure, the heavy atom compound binds asymmetrically to the dimer. Three minor heavy atom sites are located near Cys 33 (two in monomer A, one in B), whereas the main dicyanoaurate site is found near residues Phe 41–Ile 46 in monomer A only. The corresponding region in monomer B forms a short helix (α″), which is absent in monomer A. The structural asymmetry in this region is preserved in the native structure. The two monomers also differ in the N-terminal tail region, which interacts with the region near helix α″ within each monomer and might affect its conformation. As packing effects cannot be excluded, it is difficult at this stage to ascertain whether the asymmetry has biological relevance or not.

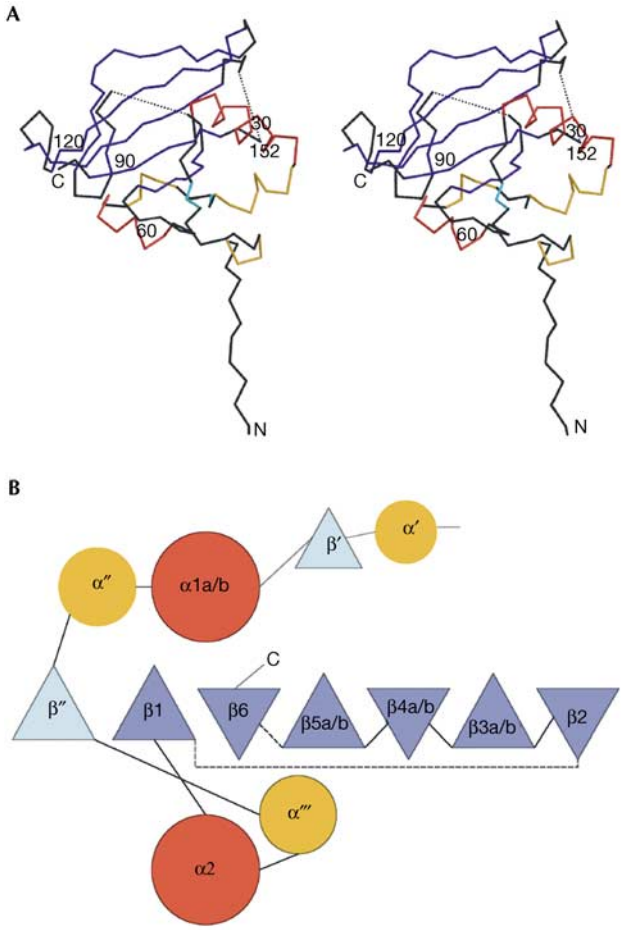

Fig 1 | ANAC NAC domain fold. (**A**) Stereo diagram showing the Cα trace of monomer B in the dicyanoaurate derivative. The secondary structure elements are colour coded as in (**B**) for clarity, and disordered regions are drawn in dashed lines. The figure was produced with MOLSCRIPT (Kraulis, 1991) and Raster3D (Merrit & Bacon, 1997). (**B**) Topology diagram of the ANAC NAC domain based on that produced by the TOPS server (Gilbert *et al*, 2001). The main antiparallel β-sheet and two helices packing against it are shown in dark blue and red, respectively, whereas extra secondary structure elements are in light blue (strands) and orange (helices). Small interruptions and irregularities are present in some of the secondary structure elements, so that helix α1 is split, for example, into α1a and α1b. The helices drawn without a border (α′ and α″) are only present in monomer B in the dimer, whereas dashed lines represent the loops that could not be traced in the structure.

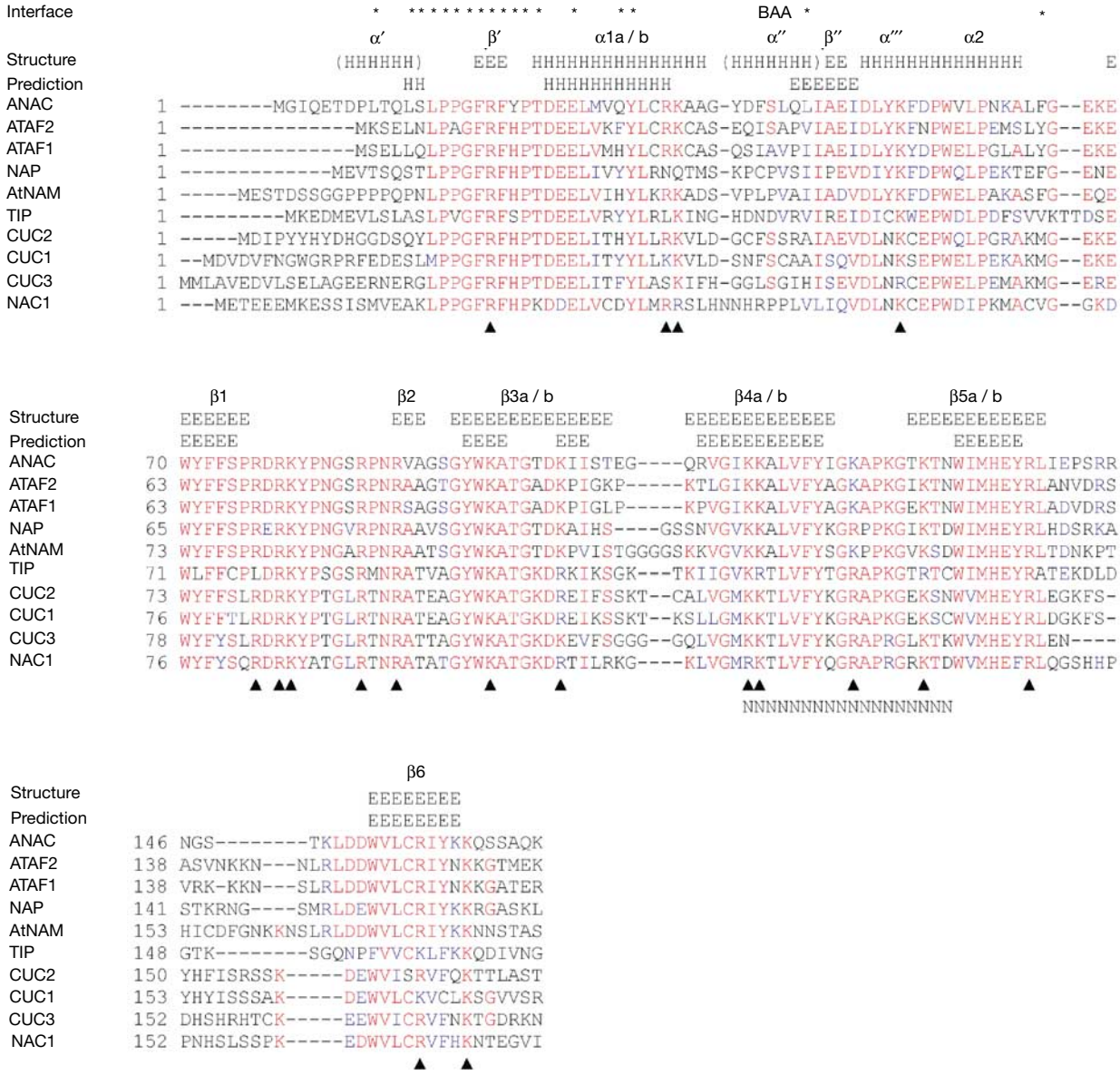

Fig 2 | Sequence alignment of ANAC and nine other NAC proteins from *Arabidopsis*. Red residues are common to at least half of the sequences, whereas blue residues are chemically similar in more than half of the sequences or similar to the dominating residue. Predicted (Greve *et al*, 2003) and observed secondary structure of the ANAC NAC domain is indicated above the alignment. H and E denote helices and strands, respectively. Secondary structural elements enclosed in parentheses are only present in monomer B. Asterisks mark residues located at the dimer interface. In the α″ region, which is different in the two monomers, residues involved in dimerization are marked with A or B. The region predicted to function as a nuclear localization signal in NAC1 and ANAC is marked by N. Triangles mark basic residues that are conserved in more than half of the sequences in the *Arabidopsis* NAC protein family. ANAC: At1g52890; NAP: At1g69490; AtNAM: At1g52880; ATAF1: At1g01720; ATAF2: At5g08790; CUC2: At5g53950; CUC1: At3g15170; CUC3: At1g76420; NAC1: At1g56010; TIP: At5g24590. Multiple sequence alignment was performed with ClustalW (Thompson *et al*, 1994), and BOXSHADE was used to produce the graphical presentation of the alignment.

DNA binding

NAC domains from the *Arabidopsis* proteins NAC1 and AtNAM have been shown to bind specifically to a fragment of the CaMV 35S promoter (Xie *et al*, 2000; Duval *et al*, 2002). The ability of the ANAC NAC domain to bind DNA was examined using *in vitro* gel mobility shift assays. As NAC proteins do not bind DNA randomly (Duval *et al*, 2002), and no biological target gene has been identified for NAC proteins, the −90 to +9 CaMV promoter fragment was used for the assays (Fig 4). The gel mobility of the labelled −90 to +9 CaMV fragment decreased by the addition of purified NAC domain, showing that the NAC domain of ANAC is also able to bind DNA. The promoter fragment contains several palindromic motifs, which could potentially be the binding site for a NAC domain dimer.

However, no well-known DNA-binding motif (Müller, 2001) could be identified in the domain. Duval *et al* (2002) analysed

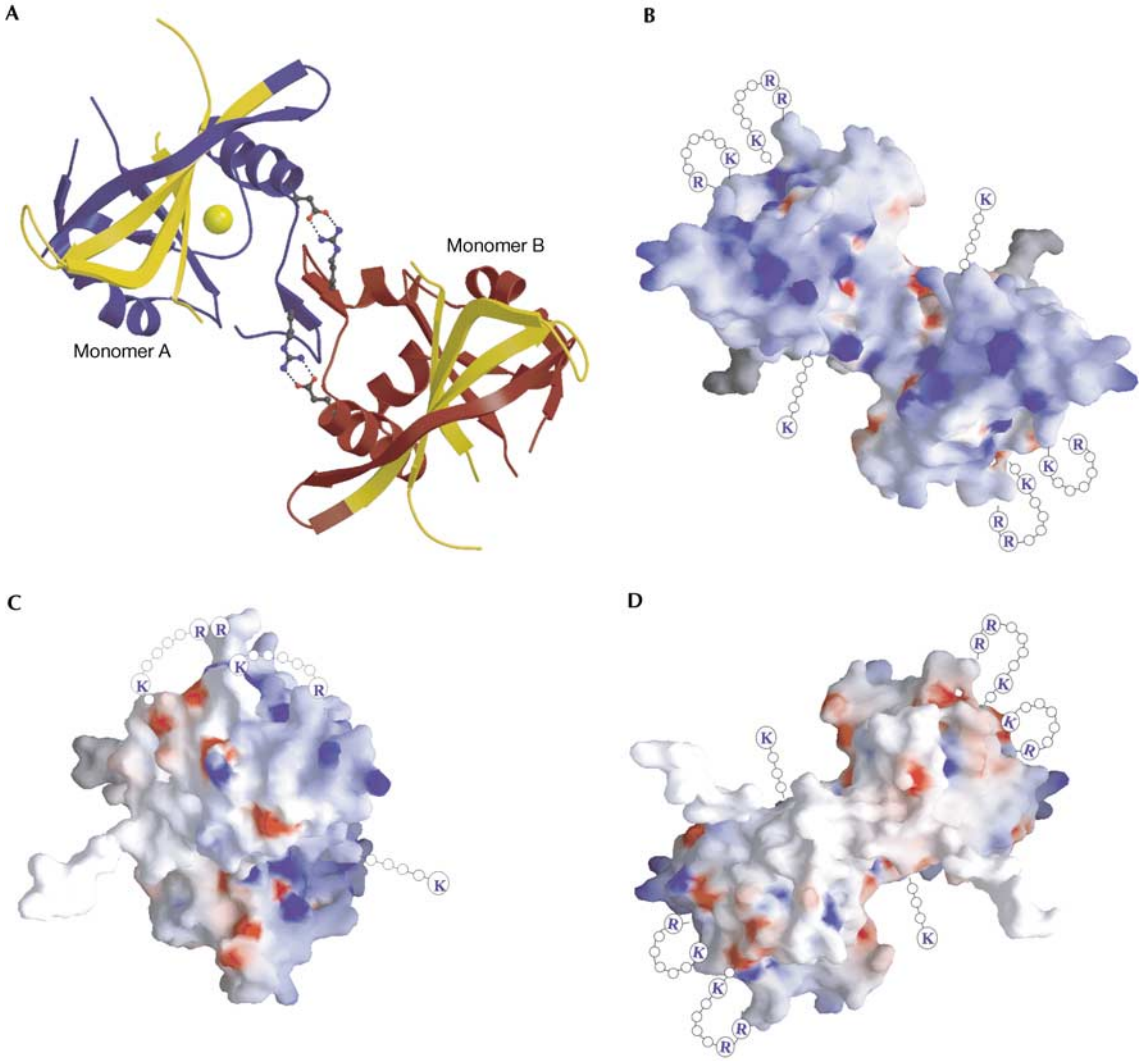

Fig 3 | Functional NAC dimer in the 1.9 Å dicyanoaurate derivative structure. (**A**) Cartoon representation of the dimer (excluding the first 11 residues in monomer A and nine in monomer B in the disordered N-terminal tail region). The salt bridges between the conserved residues are shown. The two monomers are shown in blue and red, whereas the region responsible for DNA binding according to Duval *et al* (2002) is shown in yellow. The main dicyanoaurate site is displayed as a sphere. The figure was produced with MOLSCRIPT (Kraulis, 1991) and Raster3D (Merrit & Bacon, 1997). (**B–D**) Surface representations of the NAC dimer in different views (**B**) is in the same orientation as (**A**), while (**C**) and (**D**) correspond to clockwise rotations of 90° (**C**) and 180° (**D**) around a central vertical axis lying in the plane of the paper. Positive (blue) and negative (red) charges are mapped onto the surface. The charged residues in regions missing in the model (loops between β1 and β2 and β5 and β6, and the C-terminus) are represented schematically. The figure was produced with GRASP (Nicholls *et al*, 1991).

AtNAM deletion mutants in yeast for their ability to bind the CaMV promoter fragment, and reported that the region corresponding to ANAC residues Val 111–Lys 168 constitutes the DNA-binding domain of the AtNAM protein. On the basis of secondary structure predictions, they hypothesized that the region would fold into a helix–turn–helix structure. The region from Val 111 to Gln 163 (five residues could not be traced at the C-terminus) is shown in yellow in Fig 3A. It consists of β-strands 4, 5 and 6 and the connecting turns, evidently not a helix–turn–helix structure. The only NAC domain region that might be reminiscent of the motif is helices α1a/b and α″ in monomer B. However, the α1–α″ region of the ANAC sequence has four acidic residues and only two basic residues, and is thus not likely to form a DNA-binding motif. Furthermore, the sequence forming α″ is not well conserved in NAC proteins. Surface representations showing the charge distribution on the NAC dimer are presented in Fig 3B–D. It is apparent that one face is rich in positive charges, whereas the other is not. The extremities of β-strands 4 and 5 and the connecting turn protrude from the face of the NAC dimer that is rich in positively charged residues. As this area of the structure is part of the region designated as DNA binding by Duval *et al* (2002), it is tempting to speculate that it is involved in the interaction with DNA. From alignments of NAC primary sequences, it is apparent that the area between Arg 76 and Arg 138 (ANAC numbering) is particularly rich in conserved, basic residues (see labelling in Fig 2). This corresponds to β1, β2, β3a/b,

β4a/b and β5a/b in the NAC domain structure, and thus encompasses the protruding β-'arm' and a major part of the twisted β-sheet. A number of proteins use β-sheet structures for DNA binding (Luscombe *et al*, 2000). There are several examples of two-stranded β-sheets that bind in either the major or the minor groove (Tateno *et al*, 1997). Other modes of DNA recognition by β-sheets include the three-stranded β-sheet of the GCC-box binding domain (Allen *et al*, 1998) and the five-stranded β-sheet of the GCM domain, in which the edge of the β-sheet protrudes into the major groove (Cohen *et al*, 2003). Considering the extent of the NAC domain area that is rich in conserved, basic residues, a number of modes of DNA interaction can be envisioned. It will be interesting to determine whether the NAC domain adds to the diversity of ways in which β-sheets mediate DNA binding.

Nuclear localization signals

The control of nuclear localization is pertinent to the proper function of many transcription factors. Two NAC proteins, NAC1 and ANAC, have been shown to locate to the nucleus (Xie *et al*, 2000; Greve *et al*, 2003), but no nuclear localization signal (NLS) has been experimentally identified.

Table 1 | Analysis of the dimer interface by the Protein–Protein Interaction Server (http://www.biochem.ucl.ac.uk/bsm/PP/server)

Interface parameter	Value
Accessible surface area, interface A–B (accessible surface area from A buried in the dimer)	811.4 Å^2
Accessible surface area, interface B–A (accessible surface area from B buried in the dimer)	735.2 Å^2
% of monomer accessible surface area, interface A–B	8.0
% of monomer accessible surface area, interface B–A	7.5
% polar atoms in interface A–B	30.4
% polar atoms in interface B–A	24.2
% nonpolar atoms in interface A–B	69.6
% nonpolar atoms in interface B–A	75.8
Hydrogen bonds	12
Salt bridges	2
Disulphide bonds	0
Bridging water molecules	2

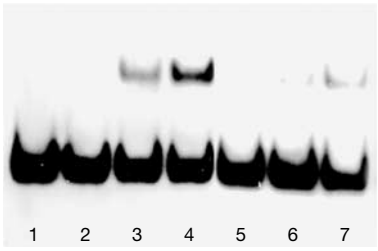

Fig 4 | Interactions of recombinant ANAC(1–168) with the −90 to +9 fragment of the CaMV 35S promoter. Lane 1, no ANAC(1–168); lane 2, 10 ng ANAC(1–168); lane 3, 50 ng ANAC(1–168); lane 4, 100 ng ANAC(1–168); lanes 5–7, same as lanes 2–4 but containing 250-fold of unlabelled −90 to +9 CaMV 35S fragment.

On the basis of sequence analysis, NAC1 has been predicted to contain a basic bipartite NLS, and the corresponding region in the ANAC sequence has been suggested to constitute a degenerate bipartite NLS (Xie *et al*, 2000; Greve *et al*, 2003). The first two residues of the predicted NLS region (marked in Fig 2), Lys 114 and Lys 115, are located on β-strand 4 and are thus partly buried in the structure. The basic residues constituting the C-terminal part of the predicted NLS are, conversely, exposed at the surface. The role of the predicted NLS region in nuclear import of NAC proteins needs further investigation by mutagenesis and localization studies. The structure presented here can aid the design and interpretation of such studies.

CONCLUSIONS

In recent years, the importance of NAC proteins in plant development, transcription regulation and regulatory pathways involving protein–protein interactions has been increasingly recognized. The structure determination of the N-terminal domain of ANAC provides the first structural template for a NAC domain. We show that the NAC domain adopts a novel fold for a transcription factor, consisting of a twisted antiparallel β-sheet sandwiched between two helices. The structure suggests that this domain mediates dimerization of the NAC proteins through conserved interactions including a salt bridge, and DNA binding through the NAC dimer face rich in positive charges.

METHODS

Crystallization and structure determination. The NAC domain of ANAC was recombinantly produced in *Escherichia coli* and

Table 2 | Data collection statistics

	Native	$KAu(CN)_2$	TMLA	EMTS	K_2PtCl_4
Resolution range (Å)	30–2.50 (2.64–2.50)	30–1.90 (2.00–1.90)	30–3.00 (3.16–3.00)	30–3.00 (3.16–3.00)	30–3.50 (3.69–3.50)
Completeness (%)	95.6 (89.8)	97.9 (95.1)	99.9 (99.9)	99.9 (99.9)	99.3 (99.3)
$\langle I/\sigma(I)\rangle$	5.6 (2.5)	6.1 (2.3)	8.7 (4.7)	6.8 (2.4)	5.1 (2.4)
R^a_{merge}	0.094 (0.300)	0.061 (0.307)	0.072 (0.154)	0.097 (0.296)	0.121 (0.266)
Number of sites[b]	–	2	2	3	2

EMTS, ethyl mercurithiosalicylate; TMLA, trimethyl lead acetate. Numbers in parentheses refer to the highest resolution shell.
[a]$R_{merge} = \sum_{hkl}\sum_i |I(hkl)_i - \langle I(hkl)\rangle| / \sum_{hkl}\sum_i I(hkl)_i$, where $I(hkl)_i$ is the *i*th measurement and $\langle I(hkl)\rangle$ is the average intensity of symmetry-equivalent reflections.
[b]Number of heavy atom sites identified with SOLVE and used for phasing.

crystallized as described in Olsen *et al* (2004). Native and derivative data of form III crystals (as described in Olsen *et al*, 2004) were collected at 100 K at beamlines I711 at MAXLAB, Lund, Sweden ($\lambda = 1.0350$ Å) and ID29, ESRF, Grenoble, France ($\lambda = 0.9999$ Å). Form III crystals belong to space group $P2_12_12_1$ with cell parameters $a = 62.4$ Å, $b = 75.3$ Å and $c = 80.5$ Å in the dicyanoaurate derivative, from which the highest resolution data were obtained. Extensive data collection statistics have been shown previously (Olsen *et al*, 2004), and a short summary of the collected data is given in Table 2. The structure was solved by MIRAS after the identification of heavy atom sites in SOLVE (version 2.03; Terwilliger & Berendzen, 1999). Phasing in SOLVE with the number of sites specified in Table 2 gave a score of 14.8 and a figure of merit of 0.55. Further density modification and autotracing were carried out in RESOLVE (version 2.03; Terwilliger, 2000). The NCS symmetry was not identified automatically by RESOLVE, due to asymmetry in the binding of heavy atoms to the NCS-related monomers. The NCS matrix could, however, be identified manually using the information contained in the native Patterson map and the initial autotraced model. This matrix was used in subsequent density modification runs. To exploit the higher resolution of the dicyanoaurate derivative, density modification was carried out using amplitudes from this data set to the full resolution limit (1.9 Å). Approximately half of the backbone structure was autotraced by RESOLVE and then built manually in *O* (version 7.0.1; Jones *et al*, 1991) and by further autotracing with ARP/wARP (version 6.0; Perrakis *et al*, 1999). Crystallographic refinement was carried out in REFMAC5 (version 5.1.24; Murshudov *et al*, 1997). The final model includes 297 residues where regions A5–A8, A79–A85, B78–B85, 144–151 (A and B) and 164–168 (A and B) could not be traced. The final dicyanoaurate derivative model contains four heavy atom sites of which two had been identified by SOLVE. The four sites include two near Cys 33 in A, one near Cys 33 in B and one near region Phe 41–Ile 46 in A. Due to the low occupancies (0.13, 0.07, 0.10 and 0.21, respectively), only the gold atom of dicyanoaurate has been modelled. Refinement statistics are summarized in Table 3. Towards the end of the refinement, the coordinates were used to refine the structure against the native data set. To ascertain whether dimer asymmetry was also present in the native structure, a simulated annealing omit map was calculated in CNS (version 1.1; Brünger *et al*, 1998). A round of simulated annealing refinement in CNS was carried out before further refinement in REFMAC5. The native model consists of 296 residues, and the final refinement statistics are also shown in Table 3.

Gel mobility shift assay. A 100 bp fragment (−90 to +9) of the CaMV 35S promoter was amplified by PCR from pCAMBIA3300 using the following primers: 5′-TTTCAGCGTGTCCTCTCCA-3′ and 5′-ATCTCCACTGACGTAAGGG-3′. The promoter fragment was 3′ end labelled with digoxigenin (DIG) using a DIG Gel Shift Kit (Roche). DNA binding reactions contained 4 µl 5 × binding buffer (100 mM Hepes, pH 7.6, 5 mM EDTA, 50 mM $(NH_4)_2SO_4$, 5 mM DTT, 1% (w/v) Tween-20, 150 mM KCl), 1 µg poly[d(I-C)], 0.8 ng DIG-labelled DNA and the specified amounts of recombinant ANAC NAC domain in a final volume of 20 µl. In competition experiments, 0.1 µg of unlabelled promoter fragment was added. The binding reactions were incubated for 15 min at room temperature and resolved on a 10% polyacrylamide gel in TBE buffer (PAGEr Gold Precast Gels, Cambrex). Following electrophoresis, electroblotting was performed using a Hybond-N nylon membrane (Amersham Pharmacia Biotech), and chemiluminescent detection was carried out according to the instructions of the manufacturer of the DIG Gel Shift Kit (Roche).

Table 3 | Refinement and model statistics

	Native	Au data
R-factor work, free (%)	22.4, 28.1	21.2, 24.4
Number of atoms		
Protein	2,431	2,438
Heavy atoms	–	4
Solvent	70	183
Average *B*-factors (Å^2)		
Protein	23.1	24.0
Heavy atoms	–	28.7
Solvent	20.5	31.4
r.m.s.d. from ideal values		
Bond lengths (Å)	0.015	0.015
Bond angles (deg)	1.5	1.4
Torsion angles (deg)	6.8	6.7
Ramachandran plot		
Most favoured regions (%)	90.9	93.0
Additional allowed regions (%)	8.6	7.0
Generously allowed regions (%)	0.4	–

ACKNOWLEDGEMENTS

We thank Eva Johansson, Flemming Hansen (University of Copenhagen) and Andrew McCarthy (ESRF) for help with data collection, and MAX-LAB (Lund, Sweden) and ESRF (Grenoble, France) for synchrotron time. Travel to synchrotrons was supported through the EU 'Access to Research Infrastructures' programme and a Danish National Science Council grant to DANSYNC. H.A.E., L.L.L. and S.L. acknowledge financial support from the Danish National Research Foundation. K.S. was supported by the Danish National Research Foundation, and A.N.O. by a Ph.D. stipend from the University of Copenhagen.

REFERENCES

Aida M, Ishida T, Fukaki H, Fujisawa H, Tasaka M (1997) Genes involved in organ separation in *Arabidopsis*: an analysis of the *cup-shaped cotyledon* mutant. *Plant Cell* **9:** 841–857

Allen MD, Yamasaki K, Ohme-Takagi M, Tateno M, Suzuki M (1998) A novel mode of DNA recognition by a β-sheet revealed by the solution structure of the GCC-box binding domain in complex with DNA. *EMBO J* **17:** 5484–5496

Brünger AT *et al* (1998) Crystallography & NMR System: a new software suite for macromolecular structure determination. *Acta Crystallogr D* **54:** 905–921

Cohen SX, Moulin M, Hashemolhosseini S, Kilian K, Wegner M, Müller CW (2003) Structure of the GCM domain–DNA complex: a DNA-binding domain with a novel fold and mode of target site recognition. *EMBO J* **22:** 1835–1845

Collinge M, Boller T (2001) Differential induction of two potato genes, *Stprx2* and *StNAC*, in response to infection by *Phytophthora infestans* and to wounding. *Plant Mol Biol* **46:** 521–529

Duval M, Hsieh T-F, Kim SY, Thomas TL (2002) Molecular characterization of *AtNAM*: a member of the *Arabidopsis* NAC domain superfamily. *Plant Mol Biol* **50:** 237–248

Gilbert D, Westhead D, Viksna J, Thornton J (2001) A computer system to perform structure comparison using TOPS representations of protein structure. *Comput Chem* **26:** 23–30

Greve K, La Cour T, Jensen MK, Poulsen FM, Skriver K (2003) Interactions between plant RING-H2 and plant-specific NAC (*NAM/ATAF1/1/CUC2*) proteins: RING-H2 molecular specificity and cellular localization. *Biochem J* **371:** 97–108

Holm L, Sander C (1993) Protein structure comparison by alignment of distance matrices. *J Mol Biol* **233:** 123–138

Hoth S, Morgante M, Sanchez J-P, Hanafey MK, Tingey SV, Chua N-H (2002) Genome-wide gene expression profiling in *Arabidopsis thaliana* reveals new targets of abscisic acid and largely impaired gene regulation in the *abi1-1* mutant. *J Cell Sci* **115:** 4891–4900

Jones TA, Zou J-Y, Cowan SW, Kjeldgaard M (1991) Improved methods for building protein models in electron density maps and the location of errors in these models. *Acta Crystallogr A* **47:** 110–119

Kraulis PJ (1991) MOLSCRIPT: a program to produce both detailed and schematic plots of protein structures. *J Appl Crystallogr* **24:** 946–950

Luscombe NM, Austin SE, Berman HM, Thornton JM (2000) An overview of the structures of protein–DNA complexes. *Genome Biol* **1**, reviews001

Merrit EA, Bacon DJ (1997) Raster3D photorealistic molecular graphics. *Methods Enzymol* **277:** 505–524

Müller CW (2001) Transcription factors: global and detailed views. *Curr Opin Struct Biol* **11:** 26–32

Murshudov GN, Vagin AA, Dodson EJ (1997) Refinement of macromolecular structures by the maximum-likelihood method. *Acta Crystallogr D* **53:** 240–255

Nicholls A, Sharp KA, Honig B (1991) Protein folding and association: insights from the interfacial and thermodynamic properties of hydrocarbons. *Proteins* **11:** 281–296

Olsen AN, Ernst HA, Lo Leggio L, Johansson E, Larsen S, Skriver K (2004) Preliminary crystallographic analysis of the NAC domain of ANAC, a member of the plant-specific NAC transcription factor family. *Acta Crystallogr D* **60:** 112–115

Perrakis A, Morris R, Lamzin VS (1999) Automated protein model building combined with iterative structure refinement. *Nat Struct Biol* **6:** 458–463

Ren T, Qu F, Morris TJ (2000) *HRT* gene function requires interaction between a NAC protein and viral capsid protein to confer resistance to turnip crinkle virus. *Plant Cell* **12:** 1917–1925

Riechmann JL *et al* (2000) *Arabidopsis* transcription factors: genome-wide comparative analysis among eukaryotes. *Science* **290:** 2105–2110

Souer E, van Houwelingen A, Kloos D, Mol J, Koes R (1996) The *No Apical Meristem* gene of petunia is required for pattern formation in embryos and flowers and is expressed at meristem and primordia boundaries. *Cell* **85:** 159–170

Tateno M, Yamasaki K, Amano N, Kakinuma J, Koike H, Allen MD, Suzuki M (1997) DNA recognition by β-sheets. *Biopolymers* **44:** 335–359

Terwilliger TC (2000) Maximum-likelihood density modification. *Acta Crystallogr D* **56:** 965–972

Terwilliger TC, Berendzen J (1999) Automated MAD and MIR structure solution. *Acta Crystallogr D* **55:** 849–861

The Arabidopsis Genome Initiative (2000) Analysis of the genome sequence of the flowering plant *Arabidopsis thaliana*. *Nature* **408:** 796–815

Thompson JD, Higgins DG, Gibson TJ (1994) CLUSTAL W: improving the sensitivity of progressive multiple sequence alignment through sequence weighting, positions-specific gap penalties and weight matrix choice. *Nucleic Acids Res* **22:** 4673–4680

Xie Q, Sanz-Burgos AP, Guo H, García JA, Gutiérrez C (1999) GRAB proteins, novel members of the NAC domain family, isolated by their interaction with a geminivirus protein. *Plant Mol Biol* **39:** 647–656

Xie Q, Frugis G, Colgan D, Chua N-H (2000) *Arabidopsis* NAC1 transduces auxin signal downstream of TIR1 to promote lateral root development. *Genes Dev* **14:** 3024–3036

Xie Q, Guo H-S, Dallman G, Fang S, Weissman AM, Chua N-H (2002) SINAT5 promotes ubiquitin-related degradation of NAC1 to attenuate auxin signals. *Nature* **419:** 167–170